Numerical Investigation of Blade Shape in Static Mixing

M. Heniche and P. A. Tanguy
Dept. of Chemical Engineering, Unité de Recherche sur les Procédés d'Écoulements Industriels (URPEI), Ecole Polytechnique, Montreal, Quebec H3C 3A7, Canada

M. F. Reeder and J. B. Fasano
Chemineer Incorporated, Dayton, OH 45401

DOI 10.1002/aic.10341
Published online in Wiley InterScience (www.interscience.wiley.com).

The mixing performance of the KMX and SMX static mixers have been compared using 3D high-resolution computational fluid dynamics (CFD) simulations. Although these mixers have a similar design composed of layers of blades, their blade shape is different: curved for the KMX and flat for the SMX. The flow of a Newtonian fluid in steady laminar regime has been considered as the benchmark of the study. The simulation was first validated by assessing the pressure drop vs. the number of mixer elements and the results were found to be in good agreement with experimental data. To evaluate the mixing quality, cross-section stream function, extensional efficiency, mean shear rate, residence time, intensity of segregation, stretching, and Lyapunov exponent have been selected. Analysis of the flow pattern and mixing parameters shows differences between the mixers and it appears that the curved blade is more efficient than the flat blade design at the expense of a slightly higher pressure drop. In practice, the KMX mixer should provide a higher mixing rate at high viscosity ratio than the SMX mixer. © 2004 American Institute of Chemical Engineers *AIChE J,* 51: 44–58, 2005
Keywords: CFD, laminar flow, in-line mixing, particle tracking, static mixer, KMX, SMX

Introduction

A static (also called motionless) mixer is composed of a solid structure in an open pipe. Its role is to create secondary flows to mix different fluid streams as they flow through the pipe. The generation of a transverse flow structure, ideally over the whole cross section, increases interfacial areas that are central to the mixing process. Static mixers are well established in numerous processing applications such as polymer blending, water and wastewater treatment, immiscible fluid–fluid (gas–gas, gas–liquid, or liquid–liquid) mixing and dispersion, chemical reactions, and heat and mass transfer (Thakur et al., 2003). One of the main interests of static mixing is the simplicity and the low cost of the system. Additional pumping energy, however, is required to offset the higher pressure drop in the pipe. A good motionless mixer should therefore combine low pressure drop and efficient mixing, a challenging design task.

The experimental investigation of new static mixer designs requires repeated laboratory-scale experiments, which quickly become cost ineffective and time consuming. From a theoretical perspective, very few static mixing flow situations can be tackled by analytical methods and the available studies are restricted to the so-called partitioned pipe geometry (Khakhar and Ottino, 1986). Geometries of practical interest are much more complicated, although they share many of the features of the partitioned pipe mixer, and the resulting flows are fully three dimensional. To investigate such flows, an alternative

Current address of M. F. Reeder: Dept. of Aeronautical Engineering, Air Force Institute of Technology, Wright-Patterson AFB, Dayton, OH.
Correspondence concerning this article should be addressed to M. Heniche at mourad.heniche@polymtl.ca.

approach is the use of computational fluid dynamics (CFD) analysis, where important advancements have been made recently in the development of efficient software products and methods of characterization.

In the past decade, several studies have been conducted to characterize static mixers (Avalosse and Crochet, 1997; Byrde and Sawley, 1999; Fradette et al., 1998; Li et al., 1998; Mickaily-Huber et al., 1996; Rauline et al., 1998, 2000; Zalc et al., 2002). A significant contribution is the work presented by Rauline et al. (1998), in which as many as six motionless mixers were investigated: Cleaveland (EMI), Inliner (Lightnin), ISG (Charles Ross & Son), Kenics (Chemineer), LPD (Charles Ross & Son), and SMX (Sulzer).

In all these studies, the same methodology to characterize the static mixers was used and herein is referred to as the *decoupled CFD-mixing approach*. Briefly, with this approach two steps can be distinguished. The first one, related to CFD, consists in the generation of the computational grid and computation of the flow variables: the velocity and pressure fields. The second step, related to the mixing analysis, uses the tracking of inert massless tracers entrained by the velocity field (Avalosse and Crochet, 1997). Because of the decoupling of the CFD and the mixing characterization, this methodology enables one to conduct studies for various types of fluids.

The limitation of the decoupled approach is that it does not take into account the effect of the viscosity ratio and/or the gravity ratio between the fluid streams to be mixed. The alternative approach that would account for viscosity ratio in calculations requires more sophisticated numerical models, such as multiphase CFD, which are still very limited in terms of the accuracy of the predictions.

It should be pointed out that, despite the above-mentioned limitation, a "know-how" has been developed over the years in the mixing scientific community, to characterize laminar chaotic flows in static mixers (Franjione and Ottino, 1987; Nauman, 1982; Ottino, 1989), based on distributive and dispersive properties. For easy mixing problems or with low viscosity ratio mixing, the dispersive properties are analyzed. For difficult mixing problems or with high viscosity ratio, both the dispersive and distributive properties are considered.

Dispersive mixing is characterized by the intensity of segregation introduced by Danckwerts (1952). When transposed in a CFD context, it represents a statistical measure of concentration of tracer positions over a given cross section, called a *Poincaré section*, for instance at the exit of the mixer. The residence time distribution (RTD) (Nauman, 1982; Nauman and Bufham, 1983) is another dispersive mixing criterion based on a statistical analysis of the tracer age distribution at the exit of the mixer. However, a good RTD does not guarantee good mixing (Ottino, 1989). Mean shear rate, extensional efficiency (Manas and Zloczower, 1994), stretching, and Lyapunov exponent are other criteria that can be used to evaluate the dispersive properties.

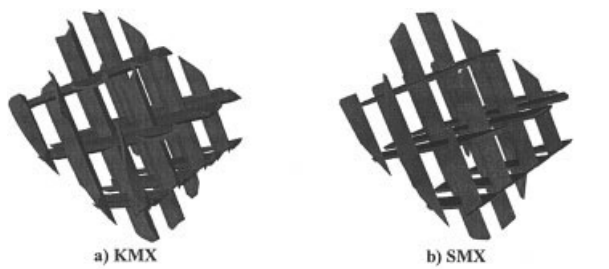

Figure 1. View of a single mixer element.

(a) KMX mixer; (b) SMX mixer.

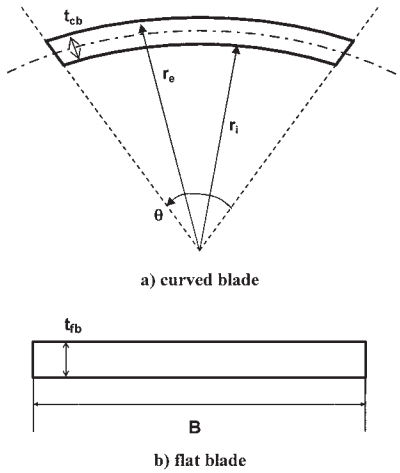

Figure 2. Definition sketch of static mixers blade cross section.

(a) KMX blade; (b) SMX blade.

In the present work, two static mixers have been compared using CFD analysis: the well-known SMX mixer (Sulzer) vs. the recently introduced KMX design (Chemineer). These mixers are very similar products (Figure 1): they share a common intricate geometry made of 24 stacked blades equally spaced arranged in two groups of 12 blades each, yielding a braided network of flow channels. The blades cross and form an angle of 90°, a value that was found to be optimal for mixing efficiency (Mickaily-Huber et al., 1996). The KMX has curved blades, with the concave surface facing upstream, whereas the SMX has flat blades (Figure 2). Both designs generate multiple fluid layers arising from flow division and reorientation that contribute to reduce the scale of the unmixed regions. As with most static mixers, each element must be rotated by 90° with respect to the previous element to give an in-line mixer device.

The objective of this work is to assess the hydrodynamic performance of the two mixers using computer simulations. One important challenge is to take into account the blade thickness in the computations. For that purpose, a high degree of numerical resolution is required. The methodology is based on the decoupled approach CFD-mixing analysis. The selected parameters used to quantify the flow pattern are the pressure drop, the mean shear rate, the extensional efficiency, and the transverse flow; and for the mixing analysis the Lyapunov exponent, the intensity of segregation, the stretching of trajectories, and the residence time. For the two mixers, a device composed of as many as 12 mixing elements ($N = 12$) has been considered (Figure 3).

KMX and SMX Blades Design

To compare the two mixers, the cross-sectional area is assumed to be equal. Expression of the blade surface area is as follows:

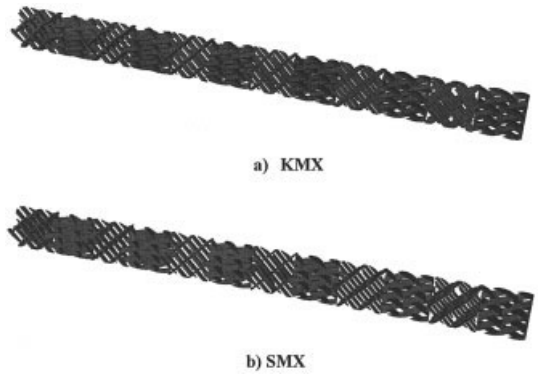

Figure 3. Motionless mixer device of $N = 12$ elements.
(a) KMX mixers; (b) SMX mixers.

$$S_{KMX} = \frac{t_{cb}}{2}\,\theta\,(r_e + r_i) \tag{1}$$

$$S_{SMX} = t_{fb}B \tag{2}$$

The parameters in Eqs. 1 and 2 are readily defined in Figure 2. From Eqs. 1 and 2, the condition of equality $S_{KMX} = S_{SMX}$ gives

$$\theta\,(r_e + r_i) = 2B\,\frac{t_{fb}}{t_{cb}} \tag{3}$$

Equation 3 will be used next in the section devoted to pressure drop analysis. Geometrical properties of the mixers used in this study can be found in Table 1.

Conditions of the Simulations

The fluid and flow characteristics used in the simulation work are presented in Table 2. They correspond to the flow of a moderately viscous Newtonian fluid in steady-state laminar regime. The governing equations are as follows

$$\text{div}\,\underline{\underline{\boldsymbol{\sigma}}} = \mathbf{0} \tag{4}$$

$$\text{div}\,\mathbf{v} = 0 \tag{5}$$

In Eq. 4, $\underline{\underline{\boldsymbol{\sigma}}}$ denotes the stress tensor, where p is the pressure, $\underline{\underline{\mathbf{I}}}$ is the identity tensor, $\underline{\underline{\dot{\boldsymbol{\gamma}}}} = 1/2[\nabla\mathbf{v} + (\nabla\mathbf{v})^T]$ is the rate of strain tensor, and μ stands for the Newtonian coefficient of dynamical viscosity.

The reference frame in the numerical model uses Cartesian coordinates (x, y, z). The pipe axis is oriented along the z-axis. The entry of the first mixer element ($N = 1$) is located at $z = 0$. The pipe cross section is defined in the x–y plane. For reasons of clarity, we may also sometimes use the cylindrical coordinate system (r, θ, z), which is more appropriate in some circumstances.

Because the z direction defines the pipe axis, the open pipe set of boundary conditions retained in the calculations is as follows:

At Inflow. The flow is imposed through a quadratic velocity profile: $u = v = 0$ and $w(r) = Q/S[1 - 4(r/D)^2]$, where Q is the flow rate, S is the empty pipe cross section, and $r = \sqrt{x^2 + y^2}$ is the radius.

At Outflow. A no-traction condition is assumed: $\underline{\underline{\boldsymbol{\sigma}}}\cdot\mathbf{n} = \mathbf{0}$, where $\mathbf{n}$ is the outward normal.

On the Rigid Wall. A no-slip condition is assumed: $\mathbf{v} = \mathbf{0}$.

The finite-element method was used for the resolution and up to 12 mixing elements were considered in the computations. The technique of periodic boundary conditions was used (for example, Rauline et al., 2000), enabling us to simulate only one element per run. The main advantage of this approach is the very high degree of mesh refinement that can be achieved, compared to modeling a whole device composed of several mixing elements with the same number of finite elements. The I-DEAS Master Series™ software (EDS) was used to generate nonisotropic unstructured 3D meshes made of tetrahedral finite elements. In practice, this meshing procedure was a formidable task because of the curved shape of the blades in the case of the KMX mixer type. Such a problem was previously mentioned for another type of static mixer in the literature (Kandhai et al., 2001; Mickaily-Huber et al., 1996). Careful attention was paid to take into account this blade curvature and the blade thickness in the calculations. First, it was not possible to generate more than one KMX element fluid model with the pipe diameter considered in the computations as well as in the mixing analysis (51.7 mm instead of 50.8 mm as indicated in Table 1) because of mesh generator limitations. Second, the number of degrees of freedom in a given static mixer exceeded the computer hardware resources available. From a practical perspective, the finer mesh used included 1.6M tetrahedral elements and 3.5M nodes for each mixer. The velocity and pressure fields were computed with a $P1^+$–P0 finite-element type (Bertrand et al., 1992), yielding over 10M equations per mixer element for SMX and KMX. The calculations for each mixer device were performed on a 64-bit IBM p690 workstation in approximately 88 h CPU time for KMX vs. 126 for SMX on a single processor using 7 GB virtual memory. It should be highlighted that, to date, such a high degree of resolution in the CFD analysis of static mixers is quite limited in the literature (Byrde and Sawley, 1999; Zalc et al., 2002).

Hydrodynamic Results

Pressure drop—validation of CFD

Pressure drop is not a measure of mixing but it is an important parameter because it governs the energy mixing costs. In this study, the pressure drop was determined to find out the effect of the blade shape on the pressure drop distribu-

Table 1. Geometrical Properties of KMX and SMX Static Mixers

Mixer	D (mm)	L (mm)	t_b (mm)	B (mm)	$\theta(r_e + r_i)$ (mm)	A (mm^2)
KMX	50.8	53.0	0.8	—	16.5	7
SMX	50.8	53.0	1.0	6.6	—	7

Table 2. Fluid and Flow Properties

ρ (kg/m^3)	μ (Pa.s)	Q (cm^3/min)	V (cm/s)	ΔP_{et} (Pa)	Re
1000	0.25	1580	1.30	2.0	3

tion. Three methods were used: (1) calculation (CFD or computational fluid dynamics), (2) experiment (EFD or experimental fluid dynamics), and (3) theory (TFD or theoretical fluid dynamics).

Let us first establish an approximate analytic relationship, under some conditions emphasized next, between pressure drops of the mixers under study. Basically, we suppose the blades to be aligned along the pipe axis; thus they do not cross. As shown in Figure 4, in a KMX or a SMX mixer element, the pipe cross section intersects 12 blades ($n_b = 12$).

In practice, for identical pipe diameter and volumetric flow rate, a difference in mixer volume results in different void fractions. Consequently, the mean velocity through the mixer would be different for the two designs. As a result, the relative pressure drop between the mixers showed to be slightly favorable to the mixer with the lower volume (and higher void fraction). The importance of each design's structural properties and manufacturing processes may, in practice, affect the mixer pressure drop. This principle can be formulated by the early Chézy law introduced at the end of the eighteenth century (Chow, 1959). Let us first express the flow rate in a pipe by

$$Q = CS^{3/2}\sqrt{\frac{\Delta P}{\chi}} \tag{6}$$

where Q is the flow rate, S is the cross flow section, C is the friction coefficient, χ is the wetted perimeter, and ΔP is the pressure drop.

At this stage, let us suppose that the flow rate, the cross section, and the friction coefficient are assumed to be identical for the two mixers; thus $Q/CS^{3/2}$ is constant. Hence, it is quite easy to deduce from Eq. 6 that the pressure drop ratio of the mixers is proportional to their blade geometry such that

$$\frac{\Delta P_{KMX}}{\Delta P_{SMX}} = \frac{\chi_{KMX}}{\chi_{SMX}} \tag{7}$$

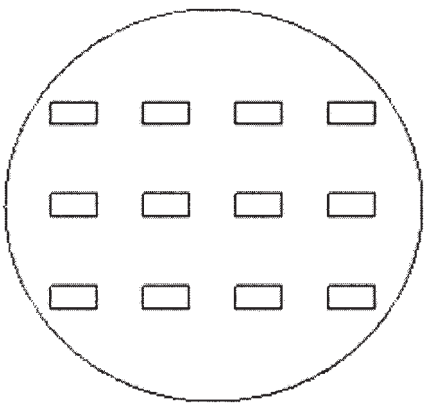

Figure 4. Typical arrangement of blades when aligned along the centerline over a cross section.

The wetted perimeter χ for the KMX mixer is defined as

$$\chi_{KMX} = \pi D + n_b[2t_{cb} + \theta(r_e + r_i)] \tag{8}$$

and for the SMX mixer as

$$\chi_{SMX} = \pi D + 2n_b(t_{fb} + B) \tag{9}$$

Introducing Eqs. 8 and 9 in Eq. 7, the following expression for the pressure drop ratio can be obtained

$$\frac{\Delta P_{KMX}}{\Delta P_{SMX}} = \frac{\pi D + n_b[2t_{cb} + \theta(r_e + r_i)]}{\pi D + 2n_b(t_{fb} + B)} \tag{10}$$

This TFD approach is simple but, as we will see in the analysis of the pressure results, it gives good predictions when compared to CFD and EFD.

As mentioned in the previous section, a serial computation by means of periodic boundary conditions technique was performed to simulate a cascade of N mixers. Thus the pressure drop over a device made of N elements is then computed from a linear combination of individual pressure drops given by the following equation

$$\Delta P = \sum_{i=1}^{N} \Delta P_i \tag{11}$$

where the subscript i stands for the mixer element number. If the flow is periodic after k elements, Eq. 11 can be rewritten as

$$\Delta P = \sum_{i=1}^{k} \Delta P_i + (N - k)\Delta P_{per} \tag{12}$$

where ΔP_{per} is the constant pressure drop per individual element mixer from the $(k + 1)$th element.

In the computation of the pressure field by CFD, special care was taken to control the effect of the mesh size because the numerical solution accuracy is mesh dependent. This is particularly critical when the geometry is as complex as that investigated herein. A particular "pathology" of CFD is the overestimation of the pressure drop when the mesh is not sufficiently refined. To address this problem, several meshes of increased resolution were generated and tested on a single mixer element ($N = 1$).

It is common to interpret the pressure drop by the dimensionless Z factor, also described in some literature studies as a "K-factor," which is expressed by the following ratio

$$Z = \frac{\Delta P}{\Delta P_{et}} \tag{13}$$

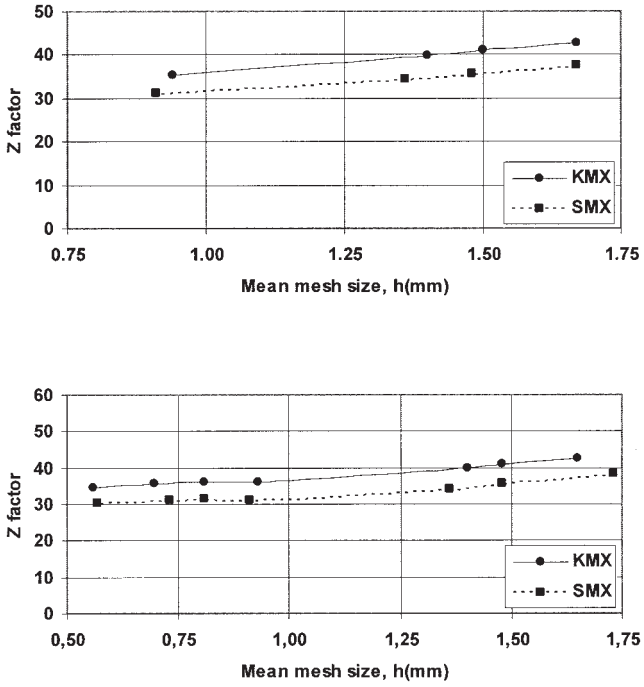

Figure 5. *Z* factor for *N* = 1 as a function of the mean mesh size *h*.

where ΔP_{et} is the pressure drop in an empty tube of equal length. The value of ΔP_{et} for a tube length equal to L is given in Table 2. Figure 5 shows plots of the nondimensional pressure drop Z factor as a function of the mean mesh size h for the two static mixers. The expression used for the determination of h is as follows

$$h = \sqrt[3]{\frac{\sum_{i=1}^{\text{NELT}} \Omega_i^e}{\text{NELT}}} \tag{14}$$

where Ω^e is the finite element volume and NELT is the total number of finite elements forming the mesh. It should be noted that mesh refinement and mesh size are inversely proportional; the number of element increases when the mesh size decreases. A significant reduction of Z was observed, about 18.6%, between the coarser (h = 1.7 mm) and the finer (h = 0.6 mm) meshes. The complete mesh independence of Z is almost achieved when $h < 1.0$ mm. The accuracy was satisfactory when compared to SMX experimental data reported in the literature (Zalc et al., 2002).

In this work, pressure drop experiments were also carried out. The experimental pressure drop was measured in a flow loop rig in which as many as six static mixing elements were inserted. The fluid was a 23 wt % polyethylene glycol (PEG) solution in water and the viscosity was 0.25 Pa·s. The flow rate control and the pressure drop measurements were monitored on a microcomputer with the LabVIEW software (National Instruments).

The pressure vs. the number of elements N is shown in Figure 6. CFD and EFD results are in good agreement. From an

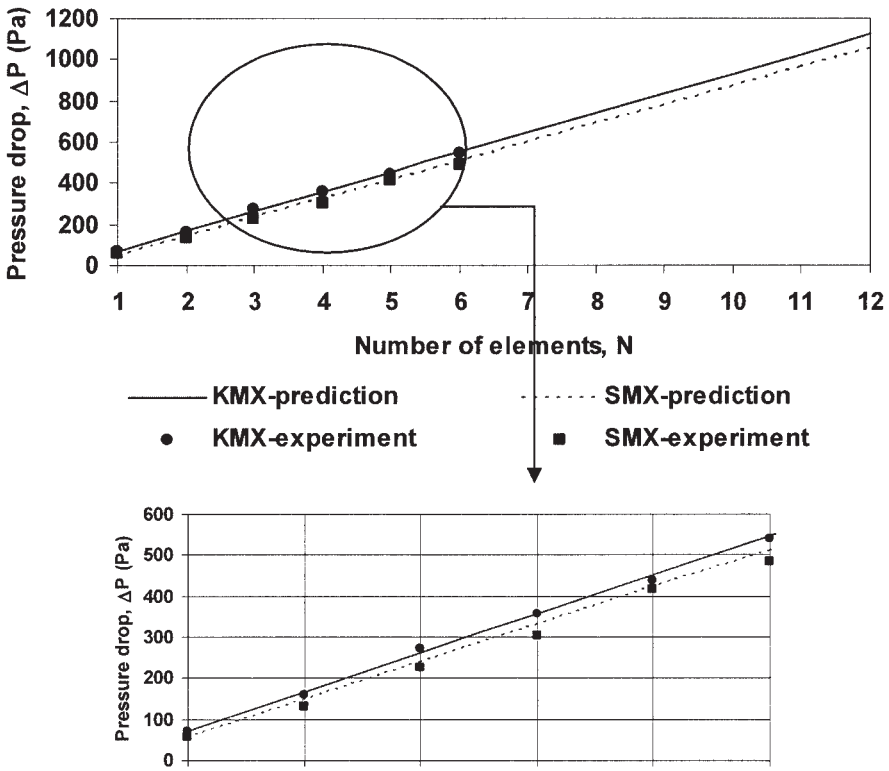

Figure 6. Pressure drop as a function of number of mixers obtained by experiment and numerical prediction for KMX and SMX devices.

Table 3. Pressure Drop Linear Regression

Mixer	CFD		EFD		
	Line Fit (Pa)	R^2	Line Fit (Pa)	R^2	$\Delta P_{CFD}/\Delta P_{EFD}$ (%) ($N = 12$)
KMX	$95.6 \times N - 25.8$	1.0000	$94.0 \times N - 22.5$	0.9979	101.7
SMX	$91.2 \times N - 30.6$	1.0000	$87.7 \times N - 37.8$	0.9968	104.9

experimental standpoint, the most important sources of uncertainties are the calibration of the flow rate (3.5%), the pressure drop gauge accuracy (2.5%), and the viscosity measurements (2.0%). Even if a detailed error analysis of the data was not performed, the difference in pipe diameter between experiment and calculation suggests an error of ±7% because the pressure drop in an open pipe varies as D^{-4} (Bird et al., 2002). In the same figure, a close-up of the experimental data is also shown for a better visual appreciation. For each mixer, the pressure drop linear fit curve and the corresponding regression coefficients, established on the basis of CFD and EFD data, are given in Table 3. Let us define the pressure drop ratios ($\Delta P_{CFD}/\Delta P_{EFD}$), where the subscripts indicate the method used to get the pressure drop. They were computed for both mixers. Their examination at high N values, which is more relevant in practice, shows that it is slightly better for KMX (101.7%) than for SMX (104.9%), 100% being the ideal situation.

In the same manner, the pressure drop ratio ($\Delta P_{KMX}/\Delta P_{SMX}$) was computed from the linear regressions presented in Table 3. Results are given in Table 4 for $N = 12$. It can be seen that the curved blade exhibits a consistent higher pressure drop. Considering the CFD, EFD, and TFD pressure drops, the ($\Delta P_{KMX}/\Delta P_{SMX}$) ratio varies in the range 5.0–10.0%. Reeder and Fasano (2001) carried out an experimental measurement of pressure drop through KMX and SMX mixers in creeping flow regime at Re = 0.03, which is two orders of magnitude lower than that of the present study. They observed a close similarity between the mixers.

As a final remark, it is worth mentioning that by reference to Eq. 12, it was found that $k = 1$ for the two mixers. In other words, the flow exhibits the periodic pressure drop ΔP_{per} just after the first mixing element.

Transverse flow

The transverse flow generated by the blades in the two static mixers is fairly tortuous, as shown in Figure 7. However, it is more the complexity of the secondary flow pattern that is of primary importance given that it improves radial mixing. A complex flow structure develops formed by several laminar eddies, no dead flow zone exists, and complete flow inversion occurs element by element over the whole cross-sectional plane. According to Table 5, the magnitude of the average transverse velocity is very close for the two mixers. However, the secondary flow is more pronounced for the curved blade when the comparison is made on the basis of the average and the maximum transverse velocities.

The two motionless mixers generate a radial fluid circulation rate Q_{sd} (subscript *sd* stands for secondary) in the x–y (or r–θ) plane in addition to the main axial flow rate Q (Figure 8). The magnitude of Q_{sd} generated by one mixing element can be estimated by the following equation

$$Q_{sd} = L \times |\Psi_{\max} - \Psi_{\min}| \tag{15}$$

where Ψ is the stream function and the subscripts min and max stand for its minimum and maximum value, respectively; and L is the characteristic length (along pipe axis) introduced to express Q_{sd} in volumetric flow units. The transverse flow vanishes rapidly (3 mm after the exit, intensity of Q_{sd} is reduced by approximately half) at the exit of the mixer device and we can consider that the transverse flow develops only within the mixer device, so that the characteristic length considered herein is equal to the length of one mixer element. Such an approximation assumes Q_{sd} to be constant over one mixer.

The estimation of Q_{sd} requires knowledge of the Ψ function, which was obtained through advanced numerical computation attributed to secondary flow complexities, impossible to determine analytically. In this work, a two-dimensional (2-D) triangular finite-element mesh was used to compute Ψ at the exit cross section of each mixer by solving the governing Poisson equation

$$\Delta\psi = \frac{\partial u}{\partial y} - \frac{\partial v}{\partial x} \tag{16}$$

Table 4. Pressure Drop Ratio

	CFD	EFD	TFD (Eq. 10)
$\Delta P_{KMX}/\Delta P_{SMX}$ (%) ($N = 12$)	104.8	109.0	110.2

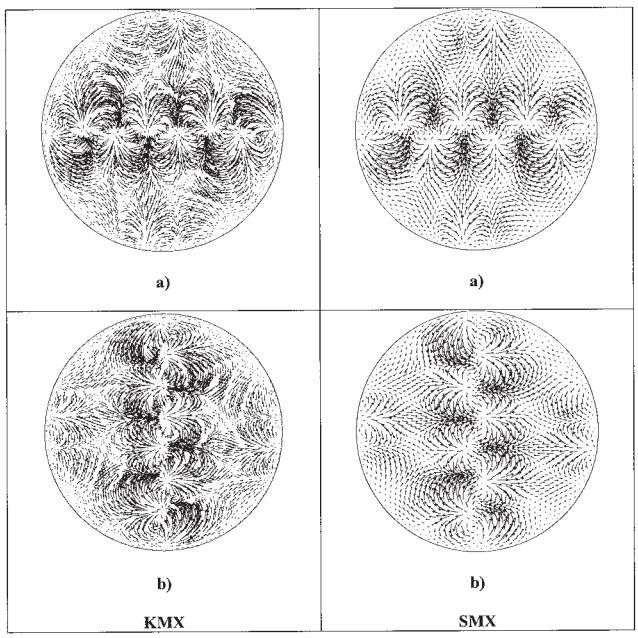

Figure 7. Transverse flow at exit of (a) odd element and (b) even element mixer.

Table 5. Transverse Flow Characteristics

	KMX	SMX
Average transverse velocity, cm/s	0.33	0.27
Maximum transverse velocity, cm/s	0.96	0.88
Transverse flow Q_{sd}^{ref}, cm^3/min (Eq. 15)	119.9	104.7
Flow ratio Q_{sd}/Q, %	7.6	6.6

In Figure 9, computed streamlines exhibit a symmetric pattern, rotated with respect to tube axis by 90° after each mixing. High density of streamlines suggests a higher transverse flow intensity in the central region.

The influence of mesh size on the accuracy of computed Q_{sd} at the exit of first element is done as well. Figure 10 presents for both mixers the variation of Q_{sd} normalized byQ_{sd}^{ref}, being the secondary flow of reference computed on the more refined mesh used, as a function of mesh size h. Mesh independence is achieved for $Q_{sd}/Q_{sd}^{ref} = 1$ when $h \rightarrow 0$. It appears clearly that SMX converges faster than KMX. One explanation for the higher uncertainty observed on KMX is that the finite-element grid might not be sufficiently refined, despite the already very large number of elements used to fit closely the curved geometry. Because of its flat blade geometry, SMX demands less effort in mesh refinement to obtain more accurate results.

In Table 5, the Q_{sd}/Q ratio is found constant at 6.6 and 7.6%, for flat and curved blades, respectively, and independent of the value of N. This is a confirmation of a faster transverse flow noticed earlier for the curved blade design. However, the blade shape does not affect the flow periodicity observed numerically on the two mixers. In other words, the solution for mixing element number $(N - 1)$ is also the solution for mixing element number $(N + 1)$. This holds true whenever $N \geq 4$.

Mean shear rate

An indication of the capability of a mixer to break up solids agglomerates, drops, and bubbles is given by the mean shear rate. Figure 11 shows the computed mean shear rate profile of the two motionless mixers along the mixer length. The number of nodes for the calculation of these shear rate distributions was chosen such that the results are mesh independent. In the figure, boxed values represent the average shear rate in the mixer.

Since the fluid under study is Newtonian and the flow is laminar, according to Eq. 4, the higher the pressure drop, the higher the shear rate. When referring to the computed pressure drop, it is thus consistent that the mean value $\bar{\gamma}_{KMX} = 7.3\ s^{-1}$ is higher than $\bar{\gamma}_{SMX} = 4.9\ s^{-1}$. Although the mean shear rate gives a good idea about shearing level, a more appropriate interpretation should be made based on the conversion of pressure drop into shearing. This is particularly useful to understand the relation between the energy loss and the entrance conditions.

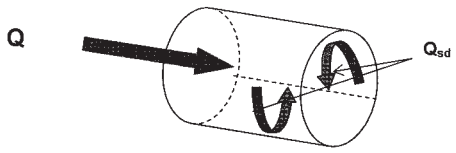

Figure 8. Schematic representation of flow components.

Flow rate (Q) and transverse flow (Q_{sd}).

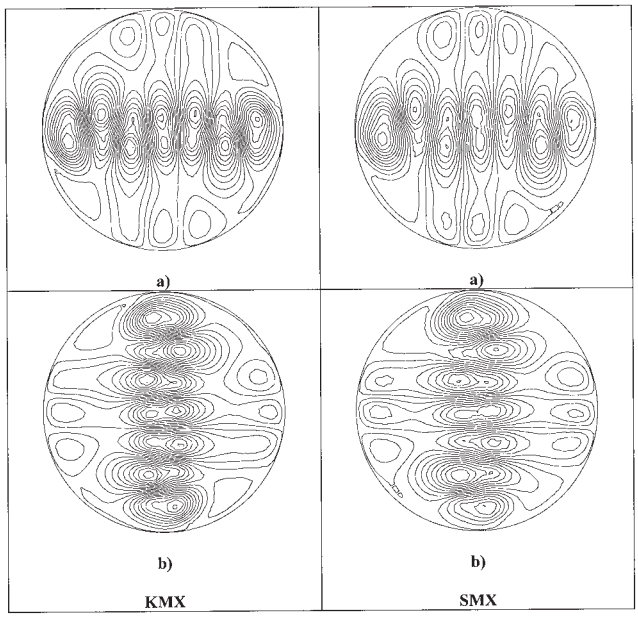

Figure 9. Streamlines at exit of (a) odd element and (b) even element mixer.

Looking again at Figure 11, it is quite evident that KMX and SMX shear rate oscillatory profiles are significantly different. At the entrance of all elements, the SMX mixer exhibits a consistent mean shear rate peak of about 8.0 s^{-1}. Into the mixer, the values range between 4.0 and 6.0 s^{-1}. In the central part of the mixer the minimum peak falls close to 3.0 s^{-1}. In comparison, the KMX exhibits a much higher shear rate along the mixer. At the entrance the peak magnitude reaches 25.0 s^{-1} over three times higher than the mean value. Into the mixer, the values range between 4.0 and 8.0 s^{-1}, reaching a maximum of 10 s^{-1} in the central part. This distinct difference in shear rate between the mixers has been already inferred by Reeder and Fasano (2001), through observation of sheets of low-viscosity additives driven along the trough of each curved blade, which are abruptly sheared by strong cross-stream velocity gradients as they eventually pass around the upstream surface.

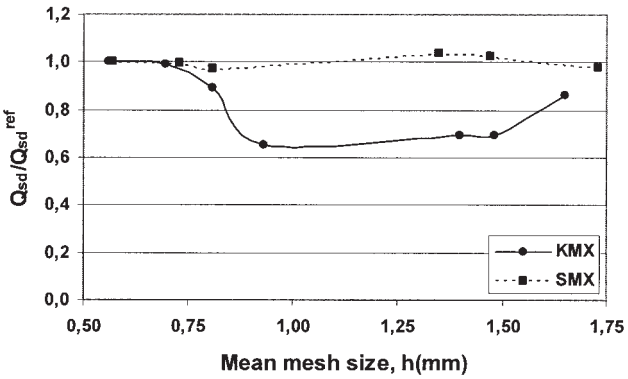

Figure 10. Normalized secondary flow as a function of the mean mesh size.

Stretching efficiency

The extensional efficiency α (Manas-Zloczower, 1994) was also investigated. Its expression is given by the following equation

$$\alpha = \frac{|\underline{\underline{\dot{\gamma}}}|}{|\underline{\underline{\dot{\gamma}}}| + |\underline{\underline{\dot{\omega}}}|} \tag{17}$$

where $|\underline{\underline{\dot{\omega}}}|$ is the norm of the vorticity tensor. The coefficient α is equal to 0 for pure rotation, 0.5 for pure simple shear flows (such as the open pipe case), and 1.0 for pure extension. Generally, increased extensional efficiency leads to better mixing. However, a high extensional efficiency in a particular region of a motionless mixer may not be an indicator of good overall mixing because the region may be segregated. That is why additional parameters were selected and are presented next to analyze in greater depth the potential of mixing of the two mixers.

It is well known that α is not invariant and therefore depends on the frame of reference. In our study, because there is only one reference frame, the criterion can be used for comparative purposes. The stretching efficiency of the two mixers is presented in Figure 12 in the same fashion as in Figure 11. The mean values of the extensional efficiency are close, 0.58 for KMX vs. 0.59 for SMX. These mean values are as high as the highest obtained by Rauline et al. (1998) on six different mixers.

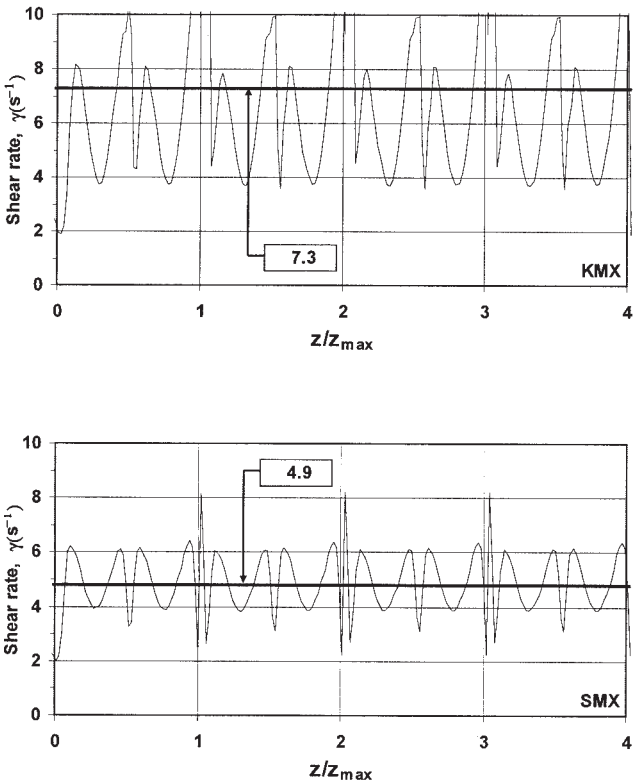

Figure 11. Shear rate.

Boxed values = mean values.

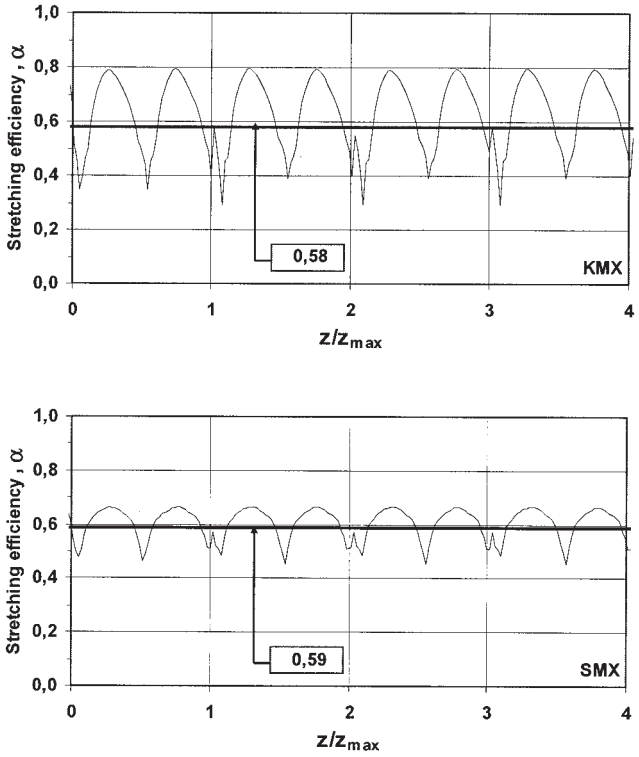

Figure 12. Extensional efficiency.

Boxed values = mean values.

Excepting entrance conditions, the shape of the α-curve follows a smooth sinusoidal signal for both mixers, although their respective magnitude are different. Indeed, the α_{KMX} magnitude varies between 0.4 and 0.8 and for α_{SMX}, between 0.5 and 0.7. This means that the curved blade causes a more varied flow than that of a flat blade according to the definition of α given above. Calculations of the stretching efficiency confirmed the previous finding in terms but did not shed any new light on the mixing performance.

Mixing Analysis

The mixing parameters retained in this study depend on the velocity field. To ease the computations, the mixing analysis has been conducted on a coarse mesh. It is well known that the velocity accuracy according to mesh size converges faster than other flow variables such as pressure or velocity derivatives (Bertrand et al., 1992). Even though not presented herein, calculations on a more refined grid show similar results.

Particle tracking

The mixing analysis presented hereafter is based on the particle tracking technique. The particles freely follow the fluid motion. The determination of a particle path is obtained by solving the following equation

$$\frac{d\mathbf{x}}{dt} = \mathbf{v}(\mathbf{x}) \tag{18}$$

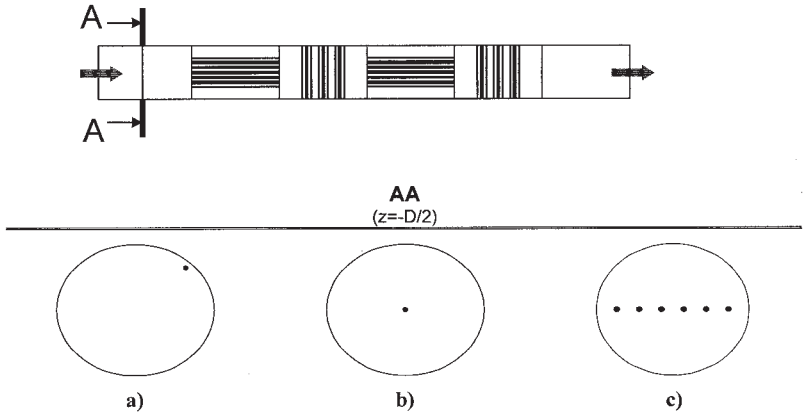

Figure 13. Conditions of injection.

(a) Off-centered; (b) centered; (c) multipoint.

where **x** denotes the vector position, **v**(**x**) is the velocity vector, and t is time. A geometrical approach was used to integrate the previous equation to obtain **x** and t because **v**(**x**) is known (Heniche and Tanguy, 2004). Figure 13 shows the position of the injection points along the centerline at $z = -D/2$. Because the choice of the injection point is often an open issue, three scenarios were investigated: off-centered ($x = y = D/3$), centered ($x = y = 0$), and "optimal" multipoint injections ($y = 0$), the latter believed to be well suited to accelerate the mixing. Positions of feed points are displayed over the cross section. On each feed point, the tracers are equally spaced (Figure 14). Figure 15 shows different views of a few computed trajectories from multipoint injection over a single KMX element. The trajectories are a good tool to visually analyze the flow transformation attributed to the presence of the mixer. In the present case, it is worthy mentioning that the trajectories within the mixer have a far richer structure compared to that of the straight lines commonly observed in an open pipe. In addition, a rapid decay of the chaotic flow behavior is observed at the exit of the mixer because the trajectories follow the open pipe particle path pattern.

Lyapunov exponent

The dynamic system theory indicates that in chaotic systems, the mixing efficiency increases with the value of the Lyapunov exponent (Ottino, 1989). The Lyapunov exponent δ is defined by the following equation

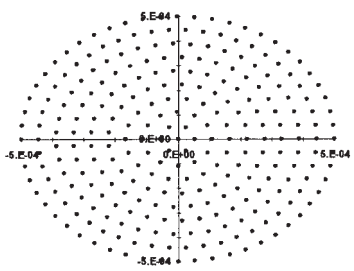

Figure 14. Typical distribution of tracers on a feed point.

$$\delta = \lim_{t\to\infty} \frac{\log \lambda}{t} \tag{19}$$

where λ is the stretching of a material line, defined as

$$\lambda = \lim_{\|dX\|\to 0} \frac{\|\boldsymbol{dx}\|}{\|\boldsymbol{dX}\|} \tag{20}$$

where $\boldsymbol{dX}$ is an initial segment and $\boldsymbol{dx}$ is the same segment stretched during a period of a sufficiently long time t. In comparison, for a laminar flow in an empty pipe (a nonchaotic system) the Lyapunov exponent is zero.

For the flow through N static mixers, the Lyapunov exponent obeys the following law (Ottino, 1989)

$$\delta = \lim_{N\to\infty}\left(\frac{1}{NT}\sum_{i=0}^{N-1} \ln \lambda_i\right) \tag{21}$$

where $T = L/V$ is the time required by the fluid to pass through a single element. Assuming that the complete mixing achieved after k mixing elements, the value of λ takes a constant value denoted λ_{per} for higher mixing elements and the Lyapunov exponent converges to $\ln \lambda_{per}/T$ for $N \gg 1$. In addition, if between the first and the kth element the $\ln \lambda_i$ values are of positive sign, then a decay of δ as a function of N may be expected.

The Lyapunov exponent was computed for the off-centered and centered injection points only. Franjione and Ottino (1987) showed that tracking of material line requires substantial computational efforts. In the calculations, we have used 132,000 segments corresponding to 1185 initial positions and 112 directions. Benettin et al. (1976) observed that the value of δ does not depend on $\boldsymbol{dX}$ as long as $\|\boldsymbol{dX}\|$ is small enough; in this study $\|\boldsymbol{dX}\| = 1$ μm was found accurate. Hereafter, we consider the Lyapunov exponent to be the average value computed among the set of all values of the stretched segments.

In Figure 16, values of averaged δ as a function of the number of mixers N are plotted for off-centered and centered

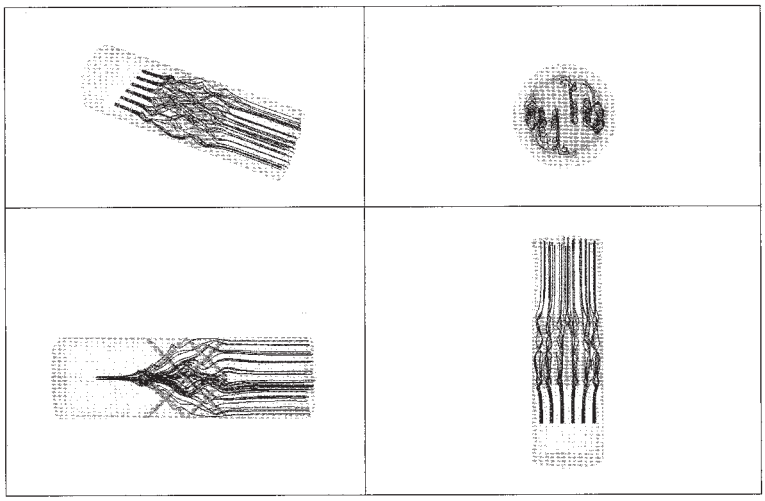

Figure 15. Different views of computed multipoint injection of particles' path over one KMX element.

injection points. Computed values of δ are of positive sign, which means that the initial filaments ***dx*** follow an exponential growth with time. Although the magnitude of the Lyapunov exponent is different for the two conditions of injection, the same scale of δ is used in the two graphs to make the comparison easier. It can be seen for the off-centered injection that the chaotic behavior of the flow can be divided in two phases. In the first one, we observe for the two mixers that δ increases with N, reaching its maximum value close to 0.3 at $N = 5$. In this phase, the flat blade gives a slightly higher chaotic behavior. On the second phase, for $N > 5$, the level of chaos is virtually identical for the two types of blades and a gradual erosion of δ is observed arising from flow periodicity.

In the case of the centered injection, the difference between the two blades is more significant and the flat blade design makes the flow more chaotic. The magnitude of the Lyapunov exponent decreases from 0.6 to 0.2, the decrease being more pronounced in the case of flat blade. The only case where δ values are equal is for $N = 12$. In Figure 16, let us consider that the Lyapunov exponent at $N = 12$ had already converged toward the following approximate plateau values 0.18 for off-centered injection and 0.20 for centered injection. According to Eq. 21 and the approximation made for high N values, the expression of λ_{per} is written as

$$\lambda_{per} \cong e^{\delta L/V} \qquad N \geq 12 \tag{22}$$

Replacing δ, L, and V in Eq. 22 by their respective numerical values, then λ_{per} reaches 2.1–2.3 for both mixers.

It is clear that a centered injection yields better performance than the off-centered injector for both mixer designs because at a given N, the values of the Lyapunov exponent are consistently higher, regardless of the type of mixer. It is worth noting that these findings are compatible with the transverse flow characteristics. We have seen from Figure 9 that over a cross section, the transverse flow is more intense (denser streamlines) in the central region, irrespective of blade type. The general transverse flow pattern is identical for the two types of blades, the only difference being the higher flow magnitude. More details can be found in Table 5.

It should be noted that other specific off-center injector locations were not investigated in this work. It would thus be premature to conclude that the investigated off-center location is representative of all other off-center configurations. Hobbs and Muzzio (1998) found considerable dependency on injector location in static mixer performance, albeit in a study dealing with a substantially different geometry.

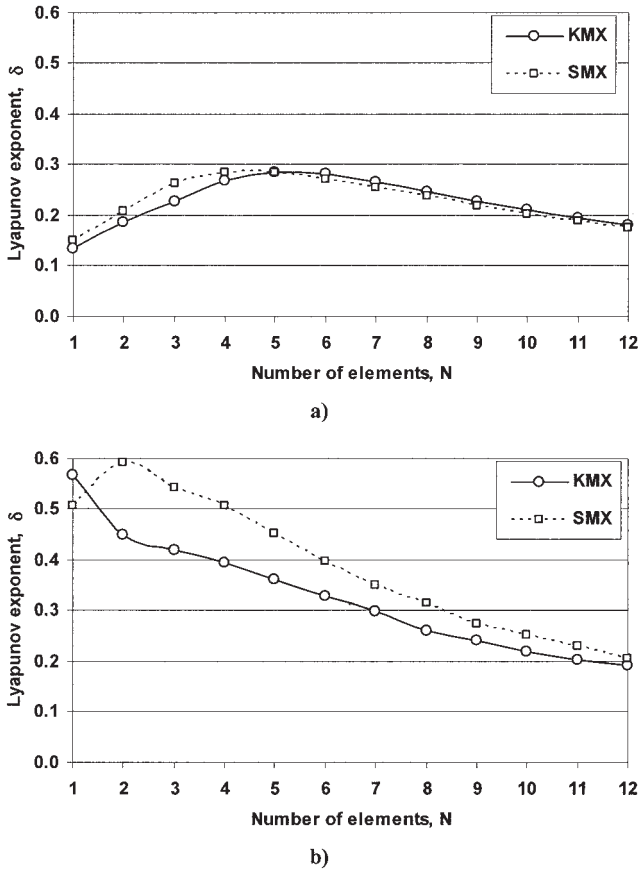

Figure 16. Lyapunov exponent for different conditions of particles injection points.

(a) Off-centered; (b) centered.

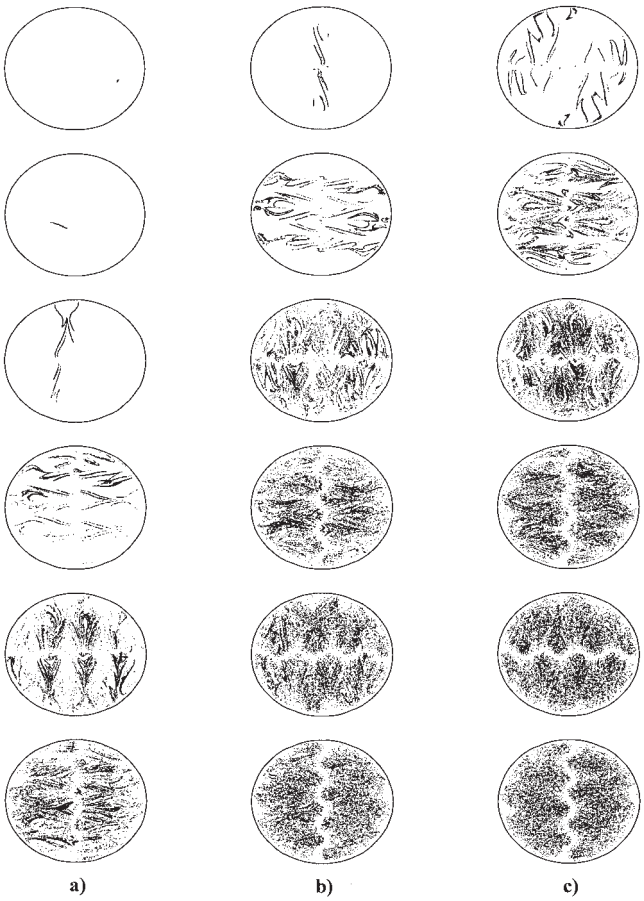

Figure 17. Poincaré sections at exit of first six (up to down) KMX elements.

(a) Off-centered injection; (b) centered injection; (c) multipoint injection.

Poincaré sections

Poincaré sections at the exit of the first six element mixers are displayed in Figure 17 for the KMX and in Figure 18 for the SMX for off-centered, centered, and multipoint injections results. For each injection scenario, six Poincaré sections are presented, the top corresponding to one element and the bottom to six elements. By looking back at the initial conditions (Figure 13), their examination shows that the particles are completely segregated. As the number N increases, the particles progressively invade the exit cross sections. Striations are still visible after six mixer elements, at least for off-centered injection, although no island or unmixed region can be noticed. Qualitatively, the off-centered is the poorest injection location and the multipoint is the best one.

To quantify the mixing from the Poincaré sections, the concept of intensity of segregation (Danckwerts, 1952) was used. The coefficient of variation COV was used to measure the intensity of segregation, that is

$$\mathrm{COV} = \frac{\sqrt{\dfrac{\sum_{i=1}^{ncells} (c_i - \bar{c})^2}{ncells - 1}}}{\bar{c}} \tag{23}$$

where c_i is the concentration of particles per unit of area in cell i, $\bar{c}$ the average concentration and *ncells* is the number of cells in the grid. COV varies between 0 (ideal distribution) and 1 (completely segregated distribution). Numerically, the COV was computed on a 10×10 triangular cell mesh from 16,000 tracers injected into the fluid.

Figure 19 shows the computed COV vs. the number of elements in a semilogarithmic plot. The three scenarios exhibit the same exponential decay toward a plateau value reached after six static mixing elements. The centered and multipoint injection locations yield the same behavior for SMX and KMX, whereas with the off-centered location the SMX appears to perform better (more rapid decrease of COV). When the number of elements is larger than six, the COV converges to 0.038 for the KMX and 0.044 for the SMX. These differences are thought to be significant in relative terms, although the absolute values are subject to the effects of discretization.

Stretching of trajectories

The stretching of trajectories, denoted Λ, was also evaluated. For periodic flows, when complete homogenization is achieved, Λ converges toward a unique value. This behavior is independent of the position of the injection point. According to Muzzio et al. (1991), the greater the stretching, the higher the

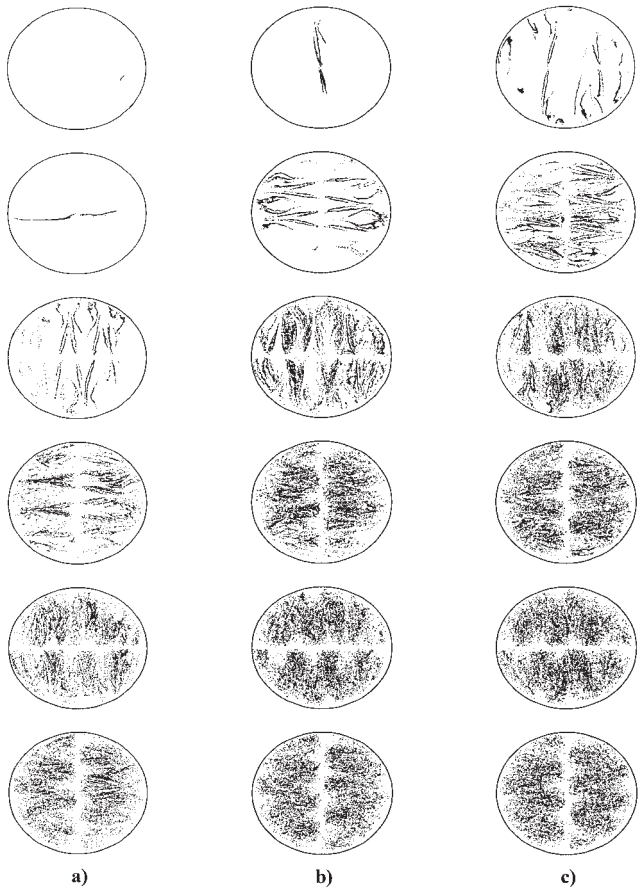

Figure 18. Poincaré sections at exit of the first six (up to down) SMX elements.

(a) Off-centered injection; (b) centered injection; (c) multipoint injection.

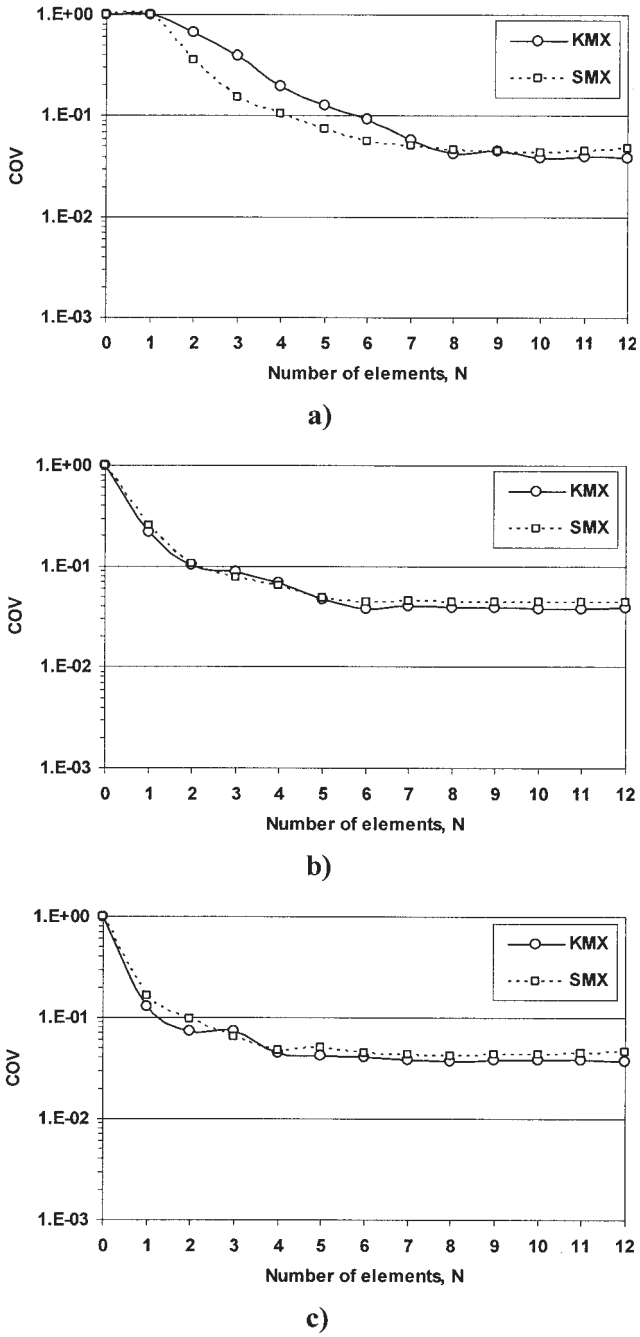

Figure 19. COV curves for different injection locations.

(a) Off-centered; (b) centered; (c) multipoint.

interfacial area and the better the contact between the phases to be mixed. In an empty pipe the trajectories of particles injected in a laminar flow are parallel and have an identical invariant length denoted $s_{ep}(\mathbf{x})$, where the subscript *ep* stands for empty pipe. For a given empty pipe, $s_{ep}(\mathbf{x})$ is known because it is equal to the pipe length. Let us consider now that a static mixer is inserted in this pipe. The property changes such that the length $s(\mathbf{x})$ of the trajectories can increase only as a result of flow obstruction. We thus define the stretching Λ of a particle trajectory by the following ratio

$$\Lambda = s(\mathbf{x})/S_{ep}(\mathbf{x}) \qquad \text{with } \Lambda \geq 1 \tag{24}$$

Figure 20 shows the mean trajectory stretching vs. the number of mixer elements. For the three conditions of injection, an interesting feature is the convergence toward a unique plateau value, which depends on the mixer type. The mean values $\bar{\Lambda}$ of Λ at convergence are 120 and 118%, respectively, for KMX and SMX. Given that $\Lambda = 100\%$ for an open pipe, this corresponds to an 11% increase of stretching in favor of the curved-blade design.

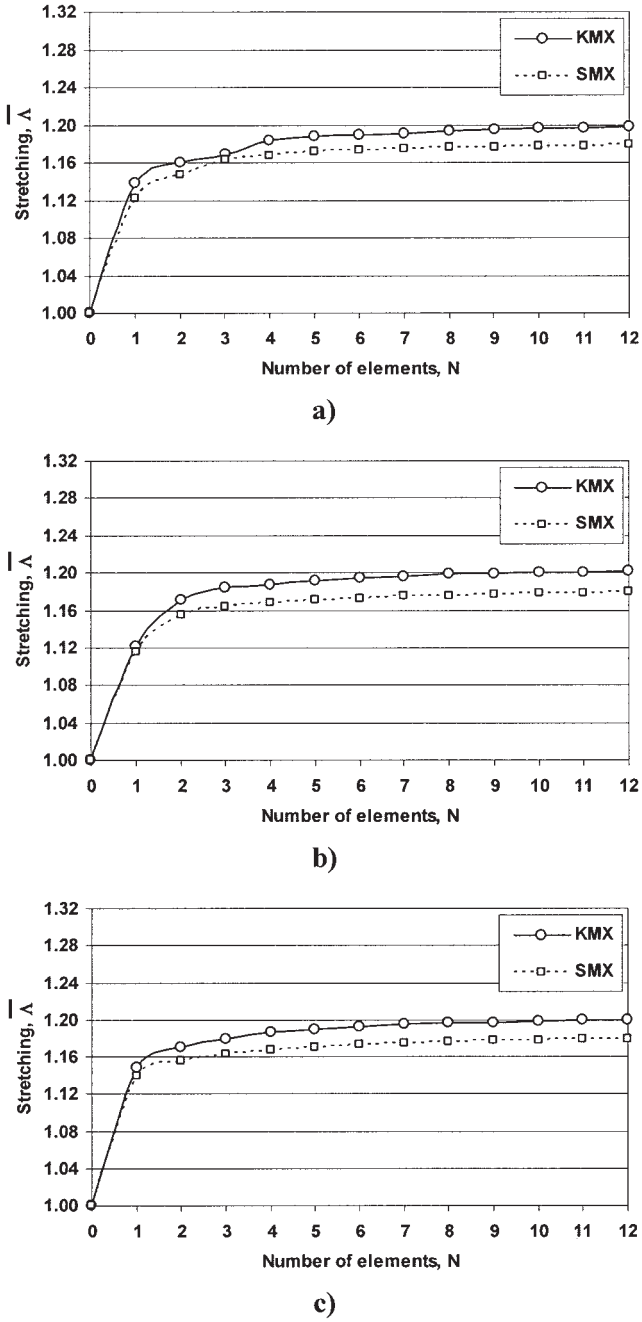

Figure 20. Stretching of trajectories curves for different injection locations.

(a) Off-centered; (b) centered; (c) multipoint.

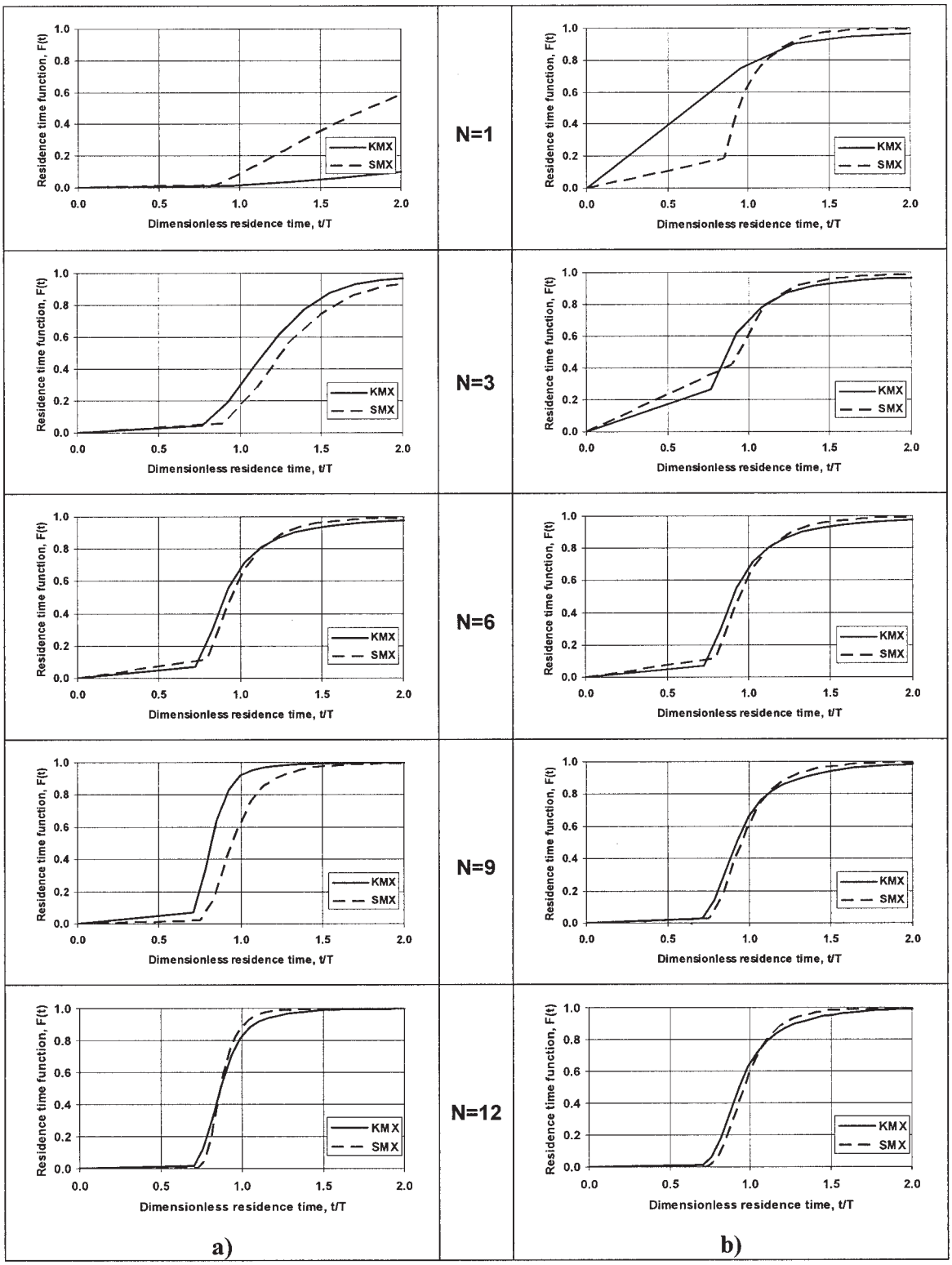

Figure 21. Residence time distribution for off-centered (a) and centered (b) injection location.

Residence time distribution

Finally, the RTD was investigated for injection of off-centered and centered particles. It is well known that the RTD is a simple method to evaluate the efficiency of mixing. According to Nauman (1982), ideal mixing for in-line mixers is obtained when the residence time function $F(t)$ is a step function, that is, when the velocity profile corresponds to a plug flow

$$F(t) = 0 \qquad 0 < t < T$$

$$F(t) = 1 \qquad t > T \tag{25}$$

where t and T, expressed in time units, represent the age of injected particles and their average age, respectively. Our evaluation of RTD is based on the Poincaré sections presented previously. This approach is similar to a pulse-input type of RTD experiment. The procedure consists in counting the particles located on the Poincaré sections at the exit of the mixers, used in defining the ranges of equal ages (in this study 50 ranges were selected) and constructing the density of the probability function $f(t)$. Integrating $f(t)$ with respect to time gives the residence time function $F(t)$. The computed $F(t)$ curves vs. the dimensionless time are presented in Figure 21 for $N = 1$, 3, 6, 9, and 12. The two mixers follow the same behavior and tend to generate a narrower distribution as N increases. Differences between the mixers are noticeable for small N values and disappear for higher values. The KMX mixer seems to achieve almost plug-flow conditions faster than the SMX for an off-centered injection. The trend is inverted in the case of a centered injection.

Final Comparison and Summary

In this study, the performance of the KMX and the SMX motionless mixers was numerically assessed. To compare the influence of the blade shape it was assumed that the wetted cross section is equal for the two mixers. The methodology of investigation was based on the decoupled CFD-mixing approach. The use of the periodic boundary condition technique enabled us to conduct simulations with a high degree of mesh refinement to study a device consisting of as many as 12 mixing elements. Several criteria were retained to compare the two designs: pressure drop, stream function, mean shear rate, stretching efficiency, Lyapunov exponent, intensity of segregation, stretching of trajectories, and residence time. The characterization showed that a difference exists between flat and curved blades in mixing a Newtonian fluid at steady state in the laminar regime.

A 3-D finite-element method was used for the determination of the flow variables. Flow periodicity was observed for the two mixers. The pressure profile analysis revealed that blade curvature is associated with a slightly higher pressure drop than that of a flat blade. This result was confirmed by EFD and TFD investigations. In addition, it was found that in the case of the curved blade, the excess of pressure drop consumption is converted into additional mixing. A complex transverse flow structure was observed at the exit of the mixers. The structure of the secondary flow is the same for the mixers but its magnitude was found to be higher for the KMX. This particularity makes the KMX slightly more chaotic. A mixing analysis was carried out based on the tracking of massless particles. Three scenarios of injection were investigated. Poincaré sections showed that the method and location of the injection substantially affected the mixture quality within the first six elements. However, computed COV showed that the two mixers achieve homogenization after six elements, irrespective of the location of injection point.

The question arises as to whether these mixers are really different. In this study, it was observed that for high N devices ($N > 6$) homogenization is obtained with the same number of mixer elements. However, in terms of mixing, the mean shear rate, the next parameter in importance to consider when mixing streams have high viscosity ratio, it appears that the curved blade is more efficient than the flat blade design at the expense of a slightly higher pressure drop. In practice, the KMX mixer should provide a higher mixing rate in viscous mixing applications. Calculations of the Lyapunov exponent as well as the mixer COV bolster this general conclusion.

Acknowledgments

This research was funded by the National Science and Engineering Research Council of Canada (NSERC) and the Pulp and Paper Research Institute of Canada (PAPRICAN). The technical help of Alfa Arzate and Olivier Reglat for the experimental work is gratefully acknowledged. Finally, the authors take this opportunity to thank one of the unknown referees for his (her) careful review of the manuscript.

Notation

A = cross blade section, mm^2
B = blade width, mm
$\bar{c}$ = mean pseudo-concentration
c_i = pseudo-concentration of tracers in cell i
D = static mixer internal diameter, mm
$F(t)$ = residence time function (between 0 and 1)
h = mean mesh size, mm
$\underline{\underline{\mathbf{I}}}$ = identity tensor
$\bar{L}$ = length of individual mixing elements, mm
N = number of motionless mixers
n_b = number of blades
p = pressure, Pa
P = mean pressure over pipe cross section, Pa
Q = volumetric flow rate, cm^3/min
R = hydraulic radius, mm
r_e = external radius of curved blade, mm
r_i = internal radius of curved blade, mm
T = period, s
t = time, s
t_{cb} = curved blade thickness, mm
t_{fb} = flat blade thickness, mm
S = pipe cross section, mm^2
$s(\mathbf{x})$ = length of particle trajectory, mm
$\mathbf{v}(u, v, w)$ velocity vector, cm/s
V = mean velocity, cm/s
$W(t)$ = washout function (between 0 and 1)
x, y, z = Cartesian coordinates, mm
Z = pressure drop ratio factor

Greek letters

α = extensional efficiency
δ = Lyapunov exponent
ΔP = pressure drop, Pa
$\underline{\underline{\dot{\boldsymbol{\gamma}}}}$ = rate of deformation tensor, s^{-1}
$\bar{\dot{\gamma}}$ = mean shear rate, s^{-1}
χ = wetted perimeter, mm
Λ = stretching of trajectories
$\bar{\Lambda}$ = mean stretching of trajectories
λ = stretching of material line
μ = viscosity, Pa·s
ψ = stream function, cm^3 min^{-1} cm^{-1}
ρ = density, kg/m^3
$\underline{\underline{\boldsymbol{\sigma}}}$ = stress tensor, Pa
$\underline{\underline{\boldsymbol{\tau}}}$ = shear stress tensor, Pa
$\bar{\theta}$ = opening angle of curved blade, rad
Ω^e = finite-element volume, mm^3
$\underline{\underline{\boldsymbol{\omega}}}$ = vorticity tensor, s^{-1}

Mathematical symbols

div = divergence operator
∇ = gradient operator
Δ = Laplace operator
bold = matrix and vector

Abbreviations

CFD = computational fluid dynamics
COV = coefficient of variation (between 0 and 1)
EFD = experimental fluid dynamics
ncells = number of cells
NELT = total number of finite elements
RTD = residence time distribution
TFD = theoretical Fluid dynamics

Literature Cited

Avalosse, Th., and M. J. Crochet, "Finite-Element Simulation of Mixing: 2. Three-Dimensional Flow through a Kenics Mixer," *AIChE J.*, **43**(3), 588 (1997).

Benettin, G., L. Galgani, and J.-M. Streclyn, "Kolmogorov Entropy and Numerical Experiments," *Phys. Rev. A*, **14**, 2338 (1976).

Bertrand, F., M. Gadbois, and P. A. Tanguy, "Tetrahedral Elements for Fluid Flow Problems," *Int. J. Numer. Meth. Eng.*, **33**, 1251 (1992).

Bird, R. B., W. E. Stewart, and E. N. Lightfoot, *Transport Phenomena*, Second Edition, Wiley, New York (2002).

Byrde, O., and M. L. Sawley, "Parallel Computation and Analysis of the Flow in a Static Mixer," *Comput. Fluids*, **33**, 1251 (1999).

Chow, V. T., *Open-Channel Hydraulics*, McGraw-Hill Classic Textbook Reissue Series, New York (1959).

Danckwerts, P. V., "The Definition and Measurements of Some Characteristic Mixtures," *Appl. Sci. Res.*, **A3**, 279 (1952).

Fourcade, E., R. Wadeley, H. C. J. Hoefsloot, A. Green, and P. D. Iedema, "CFD Calculation of Laminar Striation Thinning in Static Mixer Reactors," *Chem. Eng. Sci.*, **56**, 6729 (2001).

Fradette, L., H. Z. Li, L. Choplin, and P. A. Tanguy, "3D Finite Element Simulation of Fluid through a SMX Static Mixer," *Comput. Chem. Eng.*, **22S**, 759 (1998).

Franjione, J. G., and J. M. Ottino, "Feasibility of Numerical Tracking of Material Lines and Surfaces in Chaotic Flows," *Phys. Fluids*, **30**(12), 3641 (1987).

Heniche, M., M. F. Reeder, and P. A. Tanguy, "CFD Analysis of a Laminar Flow through KMX Static Mixers," *NLGI's Spokesman*, **67**(1), 10 (2003).

Heniche, M., and P. A. Tanguy, "A Geometrical Element-by-Element Approach for Trajectory Calculations: Application to Tetrahedral Finite Elements," *Int. J. Numer. Meth. Eng.*, submitted (2004).

Hobbs, D. M., and F. J. Muzzio, "Optimization of a Static Mixer Using Dynamical Systems Techniques," *Chem. Eng. Sci.*, **53**, 3199 (1998).

Kandhai, D., D. J.-E. Vidal, A. G. Hoekstra, H. Hoefsloot, P. Iedema, and P. M. A. Sloot, "Lattice-Boltzmann and Finite Element Simulations of Fluid Flow in a SMRX Static Mixer Reactor," *Int. J. Numer. Meth. Fluids*, **31**, 1019 (1999).

Khakhar, D. V., and J. M. Ottino, "Fluid Mixing (Stretching) by Time Periodic Sequences for Weak Flows," *Phys. Fluids*, **29**(11), 3503 (1986).

Li, H. Z., C. Fasol, and L. Choplin, "Residence Time Distribution of Rheologically Complex Fluid Passing through a Sulzer SMX Static Mixer," *Chem. Eng. Commun.*, **165**, 1 (1998).

Manas-Zloczower, I., "Studies of Mixing Efficiency in Batch and Continuous Mixers," *Rubber Chem. Technol.*, **67**, 504 (1994).

Mickaily-Huber, E. S., F. Bertrand, P. A. Tanguy, T. Meyer, A. Renken, F. S. Rys, and M. Wehrli, "Numerical Simulations of Mixing in an SMRX Static Mixer," *Chem. Eng. J.*, **63**, 117 (1996).

Middleman, S., *Fundamentals of Polymer Processing*, McGraw-Hill, New York (1977).

Muzzio, F. J., P. D. Swanson, and J. M. Ottino, "The Statistics of Stretching and Stirring of Chaotic Flows," *Phys. Fluids*, **A3**, 822 (1991).

Nauman, E. B., "Reactions and Residence Time Distributions in Motionless Mixers," *Can. J. Chem. Eng.*, **60**, 136 (1982).

Nauman, E. B., and B. A. Bufham, *Mixing in Continuous Flow Systems*, Wiley-Interscience, New York (1983).

Ottino, J. M., "Mechanical Mixing Efficiency Parameter of Static Mixers," *AIChE J.*, **29**(1), 159 (1983).

Ottino, J. M., *The Kinematics of Mixing: Stretching, Chaos and Transport*, Cambridge University Press, New York (1989).

Rauline, D., J.-M. Le Blevec, J. Bousquet, and P. A. Tanguy, "A Comparative Assessment of the Performance of the Kenics and SMX Static Mixers," *Trans. IChemE*, **A78**, 389 (2000).

Rauline, D., P. A. Tanguy, J.-M. Le Blevec, and J. Bousquet, "Numerical Investigation of the Performance of Several Static Mixers," *Can. J. Chem. Eng.*, **76**, 527 (1998).

Reeder, M. F., and J. Fasano, "Characterization of Blending in Static Mixers," Communication presented at the 18th Biennial North American Mixing Forum Conference (2001).

Thakur, R. K., Ch. Vial, K. D. P. Nigam, E. B. Nauman, and G. Djelveh, "Static Mixers in the Process Industries—A Review," *Trans. IChemE*, **A81**, 787 (2003).

Zalc, J. M., E. S. Szalai, and F. J. Muzzio, "Characterization of Flow and Mixing in an SMX Static Mixer," *AIChE J.*, **48**(3), 427 (2002).

Manuscript received Jul. 4, 2003, revision received Apr. 29, 2004, and final revision received Jul. 7, 2004.